Journal of The Electrochemical Society, 2024 **171** 100534
1945-7111/2024/171(10)/100534/9/$40.00 © 2024 The Electrochemical Society ("ECS"). Published on behalf of ECS by IOP Publishing Limited.

Enhancement of Low-Temperature Cycling Performance of Lithium-Ion Batteries by use of Dual Cosolvent

Jin-Young Oh,[1] Jin-Hong Seok,[2] Da-Ae Lim,[2] Sung-Jae Lim,[1] and Dong-Won Kim[1,2,z]

[1]*Department of Battery Engineering, Hanyang University, Seoul, 04763, Republic of Korea*
[2]*Department of Chemical Engineering, Hanyang University, Seoul, 04763, Republic of Korea*

Lithium-ion batteries (LIBs) based on conventional electrolyte suffer from poor cycling performance at low temperatures due to the reduced ionic conductivity of electrolytes, sluggish charge transfer reaction, and Li plating during the charging process. Herein, we propose a dual cosolvent composed of methyl acetate (MA) and ethyl fluoroacetate (EFA). MA effectively reduced the viscosity of the electrolyte, improving the ionic conductivity at low temperatures. EFA facilitated the de-solvation of Li^+ ions and formed an anion-derived solvation structure, enabling the formation of an inorganic-rich solid electrolyte interphase on the graphite anode. Due to the synergistic effect of MA and EFA, the graphite/$LiFePO_4$ cell employing a dual cosolvent exhibited good cycling performance at low temperatures, delivering a discharge capacity of 68.7 mAh g^{-1} at −20 °C and 0.2 C and showing a capacity retention of 99.7% after 100 cycles at −20 °C and 0.33 C. Additionally, the cell exhibited an initial discharge capacity of 131.2 mAh g^{-1} at 25 °C and 1.0 C, with a capacity retention of 99.4% after 300 cycles. Our results demonstrate that liquid electrolytes containing dual cosolvent with various beneficial roles can be a promising solution for improving the low-temperature cycling performance of LIBs.

[DOI: 10.1149/1945-7111/ad88aa]

Manuscript submitted August 26, 2024; revised manuscript received September 30, 2024. Published October 29, 2024.

Supplementary material for this article is available online

Lithium-ion batteries (LIBs) are the dominant power sources in portable electronics and electric vehicles.[1–6] The electrolyte solvents used in commercialized LIBs are typically composed of linear and cyclic carbonates, such as ethylene carbonate (EC), dimethyl carbonate (DMC), and ethyl methyl carbonate (EMC).[7] In particular, EC is considered an indispensable component due to its superior ability to dissociate lithium salts and form a stable solid electrolyte interphase (SEI) and its excellent compatibility with graphite anodes.[8–10] However, its high melting point and viscosity hinder Li^+ ion transportation at low temperatures. Moreover, the strong binding of EC with Li^+ ions slows down the de-solvation kinetics during the charging process, increasing the charge transfer resistance. These ultimately lead to significant capacity fading, shortened battery life, and lithium-plating caused safety issues at low temperatures.[11–21] Consequently, using LIBs under cold conditions, such as civil, military, polar, and space applications, is severely restricted.

Hence, extensive research has been conducted on cosolvents, such as esters, lactones, nitriles, sulfates, and ethers, to overcome the limitations of EC-based liquid electrolytes at low temperatures.[22–30] Among them, esters are attracting significant attention due to their exceptionally low viscosity (<0.5 cP) and low melting point (<−80 °C), which prevent the drastic decline in the ionic conductivity of EC-based electrolytes at temperatures below −20 °C.[23–29] However, esters lack the ability to form a protective and stable SEI layer on the graphite anode, making them ineffective in preventing continuous electrolyte consumption during repeated cycles.[30–34] In addition, they cannot lower the de-solvation energy of Li^+ ions, limiting their low-temperature operations. Fluorinated esters are promising solvents to reduce the de-solvation energy because the highly electronegative fluorine atoms draw electrons away from the carbonyl group, reducing the atomic charge and lowering the binding energy between the solvent and Li^+ ions. Moreover, the lowered charge of the carbonyl group alters the solvation structure, allowing anions to participate in the solvation and forming an anion-derived SEI on the graphite surface.[35] The anion-derived SEI layer composed of LiF, Li_2O, and Li_3N is thin, stable and mechanically robust, enabling stable cycling performance even at low temperatures.[36,37] Despite these advantages, fluorinated esters have poor capability to dissociate lithium salts and suffer from reductive decomposition at low potential, negatively impacting the battery performance.

This study proposes introducing a dual cosolvent into the conventional EC-based liquid electrolyte to complement the limitations of esters and fluorinated esters while maintaining their advantages. The dual cosolvent composed of methyl acetate (MA) and ethyl fluoroacetate (EFA) promoted the de-solvation of Li^+ ions while maintaining low viscosity and high ionic conductivity at low temperatures. In addition, the changes in the solvation structure led to the production of an anion-derived robust SEI layer on the graphite anode. Due to these synergistic effects of MA and EFA, the lithium-ion cell composed of graphite anode and $LiFePO_4$ (LFP) cathode exhibited high capacities and relatively stable cycling performance at low temperatures. The enhancement of low-temperature cycling performance in the cell employing dual cosolvent was investigated by ^7Li NMR, Raman, XPS, and SEM analyses.

Experimental Methods

Materials.—EC, EMC, fluoroethylene carbonate (FEC), EFA, and lithium hexafluorophosphate ($LiPF_6$) were provided from Dongwha Electrolyte Co., Ltd. MA and N-methyl pyrrolidone (NMP) were supplied from TCI and Sigma-Aldrich, respectively. Lithium salt was vacuum dried at 90 °C for 6 h, and the organic solvents were dried using 4 Å molecular sieve before use. A polyethylene (PE) separator (thickness: 13 μm, SKIET) was used after vacuum drying at 90 °C for 12 h.

Preparation of electrolytes and electrodes.—EC and EMC were used as the fundamental components of electrolytes with 5 wt% FEC as a SEI-forming additive. MA and EFA were employed as single cosolvents or dual cosolvents for improving low-temperature cycling performance. 1.2 M $LiPF_6$ was dissolved in the mixed solvent to prepare the electrolyte. The electrolyte compositions investigated in this study are summarized in Tables I and S1. The LFP cathode was fabricated by coating the NMP slurry comprising LFP (Ecopro BM), Super P carbon (TIMCAL), and poly(vinylidene fluoride) (PVdF, Solvay) (92:4:4 by mass ratio) on the Al foil and drying under vacuum at 100 °C overnight. The active mass loading in the cathode was about 24.8 mg cm^{-2}. The graphite anode comprised of artificial graphite (S360, BTR), PVdF, and Super P carbon (91:8:1 by mass ratio) on the Cu foil. The N/P ratio of the electrodes was

---

[z]E-mail: dongwonkim@hanyang.ac.kr

Table I. Compositions of the reference electrolyte, and electrolytes containing single and dual cosolvents.

Electrolyte	Composition
Ref	1.2 M $LiPF_6$ in EC/EMC/MA/EFA (3/7/0/0 by volume) + FEC 5 wt%
ME40	1.2 M $LiPF_6$ in EC/EMC/MA/EFA (3/3/4/0 by volume) + FEC 5wt%
ME04	1.2 M $LiPF_6$ in EC/EMC/MA/EFA (3/3/0/4 by volume) + FEC 5 wt%
ME31	1.2 M $LiPF_6$ in EC/EMC/MA/EFA (3/3/3/1 by volume) + FEC 5wt%

approximately 1.15. A coin-type cell was assembled by stacking the graphite anode, PE separator, and LFP cathode and injecting the liquid electrolyte into the cell. The preparation of electrolytes/electrodes and cell assembly were conducted in a glove box (MBRAUN) filled with argon gas, maintaining the oxygen and moisture levels below 0.1 ppm.

Electrochemical measurements.—The ionic conductivity of the electrolyte was determined using an impedance analyzer (ZIVE MP1, WonATech Co., Ltd.) in the temperature range of −40 to 30 °C. Electrochemical impedance spectroscopy (EIS) of the lithium-ion cell was performed using the impedance analyzer over a frequency range from 1 mHz to 100 kHz. Galvanostatic cycling of the graphite/LFP cell was performed between 2.5 and 3.9 V using a battery tester (WBCS 3000, WonAtech Co. Ltd). Before cycling tests, all the cells underwent two pre-conditioning cycles to form stable SEI layers at 0.1 C and 25 °C. The room-temperature cycling test was conducted at 1.0 C, while the low-temperature (−20 °C and −30 °C) cycling test was carried out at 0.33 C. For the low-temperature rate capability test, the cell was charged to 3.9 V at 0.2 C and 25 °C. Following, the cell was placed in a low-temperature chamber for 12 h and subsequently discharged to 2.5 V at different C rates and low temperatures.

Characterization.—The viscosity of the electrolyte was measured using an MCR 702e viscometer at 25 °C. ^{7}Li NMR spectroscopy was conducted using a VNMRS 600 MHz spectrometer with LiCl as the reference. Raman spectra were obtained to investigate the solvation structure of electrolyte using a LabRAM HR Evolution. The chemical composition of the SEI layer formed on the graphite anode was analyzed by XPS (Thermo Fisher Scientific Inc.). The morphology of the electrodes was examined by a field-emission scanning electron microscope (FE-SEM) (Verios G4, FEI). Density functional theory (DFT) calculation was conducted to obtain the HOMO/LUMO energy levels of organic solvents and binding energies. The DFT calculation was carried out with GAMESS software using Becke's three-parameter hybrid method employing the Lee-Yang-Parr correlation functional.

Results and Discussion

We obtained the HOMO and LUMO energy levels of organic solvents by DFT calculation. As shown in Fig. S1, EFA showed lower LUMO energy level than other organic solvents (EC, EMC, and MA), indicating EFA has the lowest reductive stability. Due to the poor reductive stability and corrosive properties of EFA solvent toward graphite, FEC was added as a SEI-forming additive into the electrolyte in this study. Figure 1 shows the schematic presentation of the solvation structure and characteristics of conventional EC-based liquid electrolyte (1.2 M $LiPF_6$ in EC/EMC + FEC 5 wt%) without and with dual cosolvent. The conventional electrolyte has a strong ability to dissociate the Li salt due to the strong interactions between Li^+ ions and organic solvents. However, it exhibits poor cycling performance at low temperatures, because the electrolyte has high viscosity and slow de-solvation kinetics. It is well known that the de-solvation of Li^+ ions is a rate-determining step at low temperatures.[14] The low-temperature performance can be improved by adding a dual cosolvent, comprising of MA and EFA, with low viscosity and weak interactions with Li^+ ions. MA in the dual cosolvent can effectively reduce viscosity and thus increase the ionic conductivity at low temperatures. Meanwhile, the addition of EFA can change the solvation structure, leading to the facile de-solvation and formation of an anion-derived SEI layer on the graphite anode.

To maximize the synergistic effect of the dual cosolvent system, we tried to find the optimal composition of two cosolvents by evaluating the cycling performance of the cells employing electrolytes with different cosolvent ratios at 25 and −20 °C. The compositions of liquid electrolytes containing single (MA, EFA)

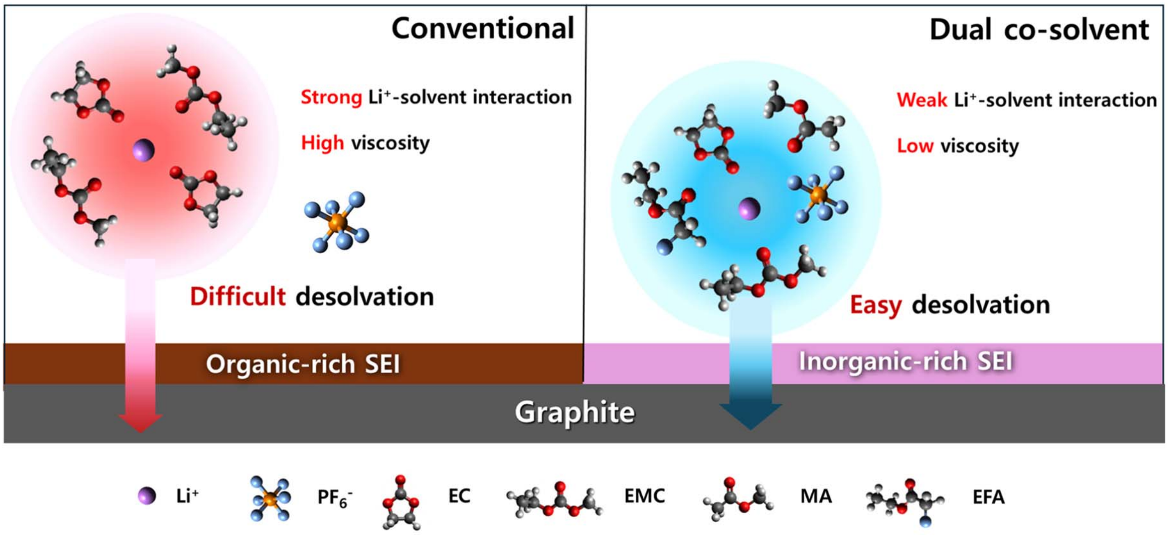

Figure 1. Schematic illustration of the solvation structure and characteristics of electrolytes without and with dual cosolvent.

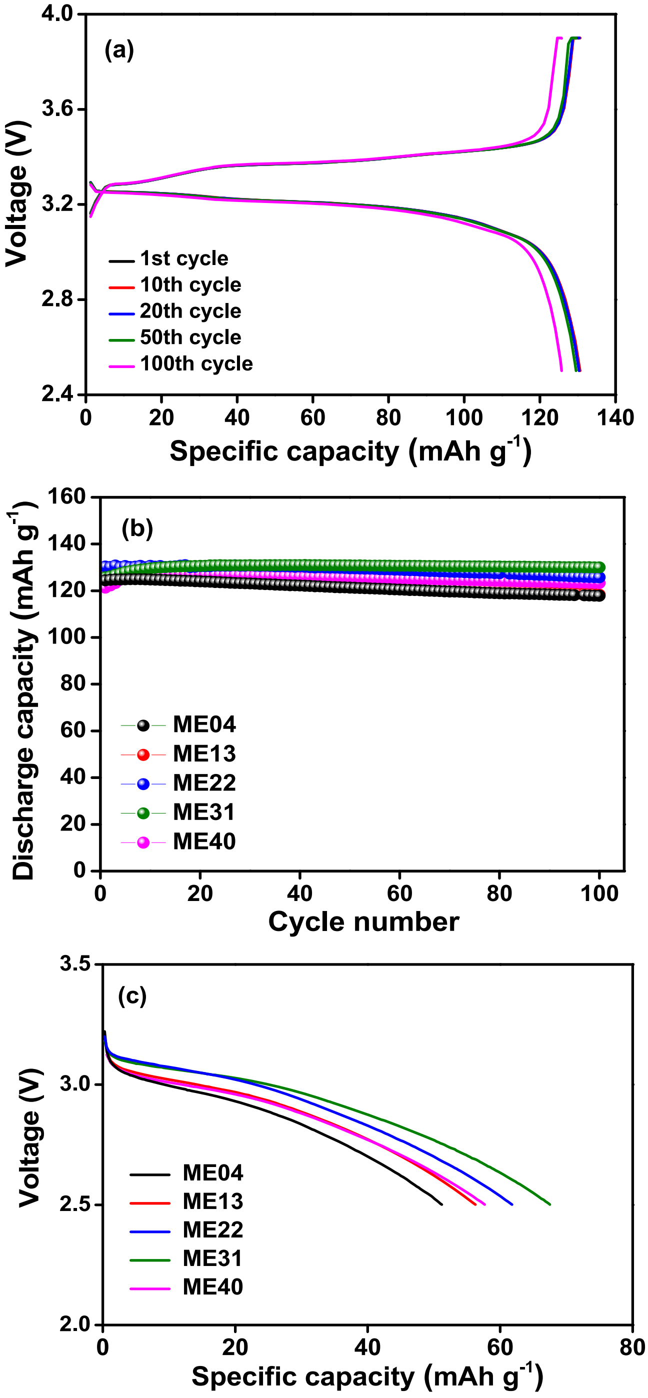

Figure 2. (a) Voltage curves of the cell employing ME22 at 1.0 C and 25 °C and (b) cycling performance of the cells with different electrolytes at 1.0 C and 25 °C. (c) Discharge curves of the cells with different electrolytes at 0.2 C and −20 °C.

or dual cosolvents (MA and EFA) are presented in Table S1. When considering cycling stability at room temperature and discharge capacity delivered at −20 °C, the cell employing ME31 (1.2 M $LiPF_6$ in EC/EMC/MA/EFA (3/3/3/1 by volume) + 5 wt% FEC) exhibited the best cycling performance, as shown in Fig. 2. Based on these results, all subsequent experiments were conducted on conventional electrolytes (Ref), electrolytes containing single cosolvent (ME40 and ME04), and electrolytes containing dual cosolvent (ME31), as listed in Table I.

The viscosities and ionic conductivities of various electrolytes investigated in this work were measured; the results are shown in Figs. 3a and 3b, respectively. The addition of MA significantly reduced viscosity compared to the Ref electrolyte. Accordingly, ME40 exhibited the lowest viscosity of 3.1 cP at 25 °C, while ME04 had a slight decrease in viscosity. Moreover, the addition of cosolvents prevented the significant drop in ionic conductivity below −20 °C. Unfortunately, adding EFA alone (ME04) decreased the ionic conductivities at temperatures above −20 °C. This is because the fluorinated ester (EFA) cannot effectively dissociate the lithium salt.[35] Except ME04, the electrolytes containing cosolvents exhibited higher ionic conductivities than Ref over all the temperature ranges. Raman and ^{7}Li NMR spectroscopy were

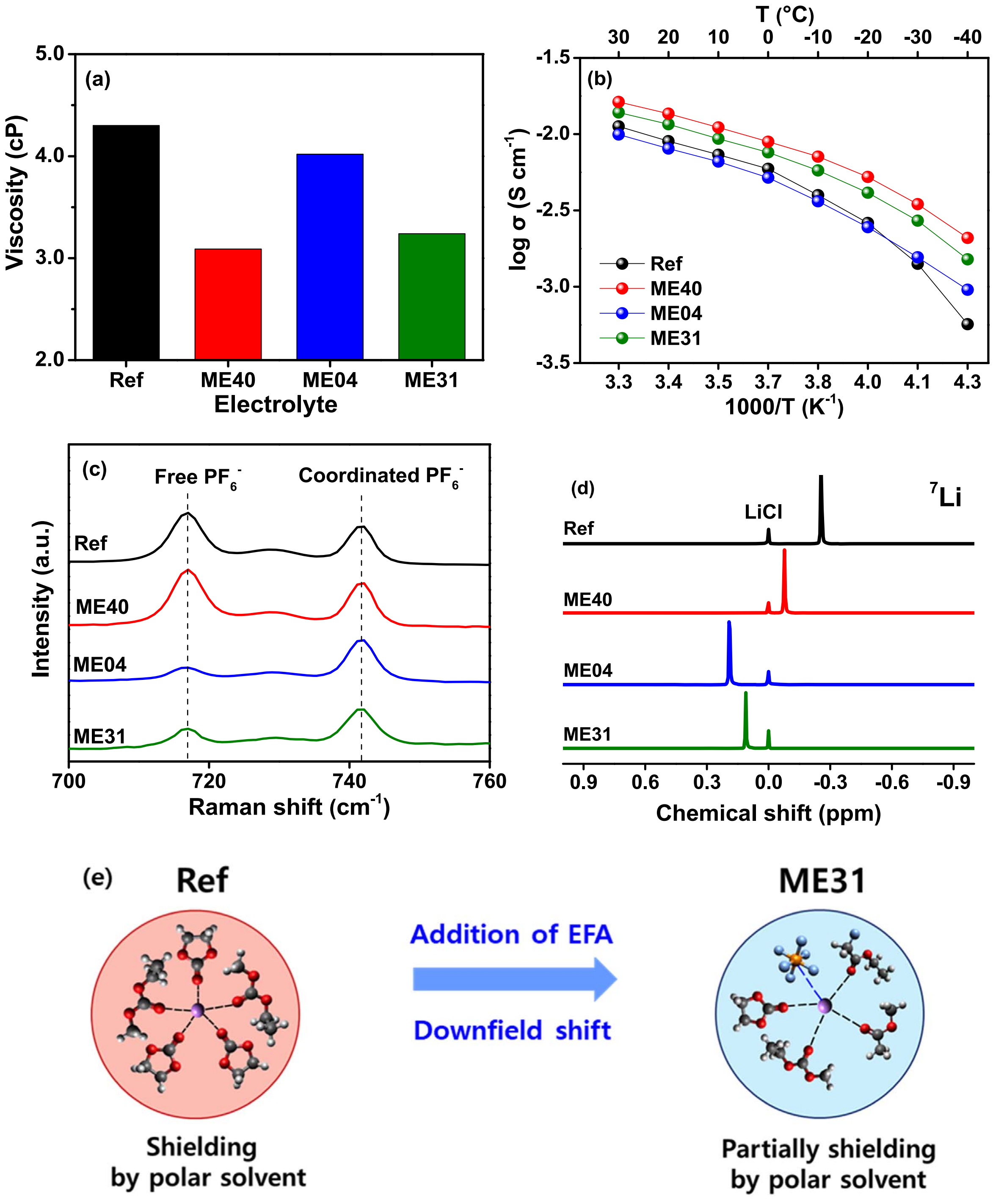

Figure 3. (a) Viscosity of different electrolytes at 25 °C and (b) ionic conductivity of different electrolytes at various temperatures. (c) Raman and (d) ^{7}Li NMR spectra of different electrolytes. (e) Variation of solvation structure with the addition of cosolvents.

conducted to understand the influence of cosolvents on the solvation structure.[38–40] As shown in the Raman spectra in Fig. 3c, all the electrolytes showed stretching vibration peaks of Li^+-coordinated PF_6^- anions at 748 cm^{-1} and the free PF_6^- anion peak at 716 cm^{-1}.[41] In the Ref and ME40 electrolytes, the peak corresponding to free PF_6^- anions appeared with high intensity, whereas its intensity was relatively weak in the ME04 and ME31 electrolytes. The reduced intensity of the free PF_6^- anion peak suggests that EFA addition promoted the formation of the Li^+-coordinated PF_6^- solvation structure rather than the complete dissociation of $LiPF_6$.

The solvation structure was further investigated using ^{7}Li NMR spectra. As shown in Fig. 3d, EFA addition resulted in the downfield shift of the ^{7}Li peak. When comparing to Ref, the degree of downfield shift was increased in the order of ME40, ME31, and ME04. This is because the presence of EFA solvent weakens the interactions between Li^+ ions and polar solvents, leading to a decrease in the electron shielding effect around Li^+ ions.[42] These results could be confirmed by comparing the binding energies between Li^+ ions and solvent, as presented in Fig. S2. It revealed that EFA solvent showed the lowest binding energy (−1.86 eV)

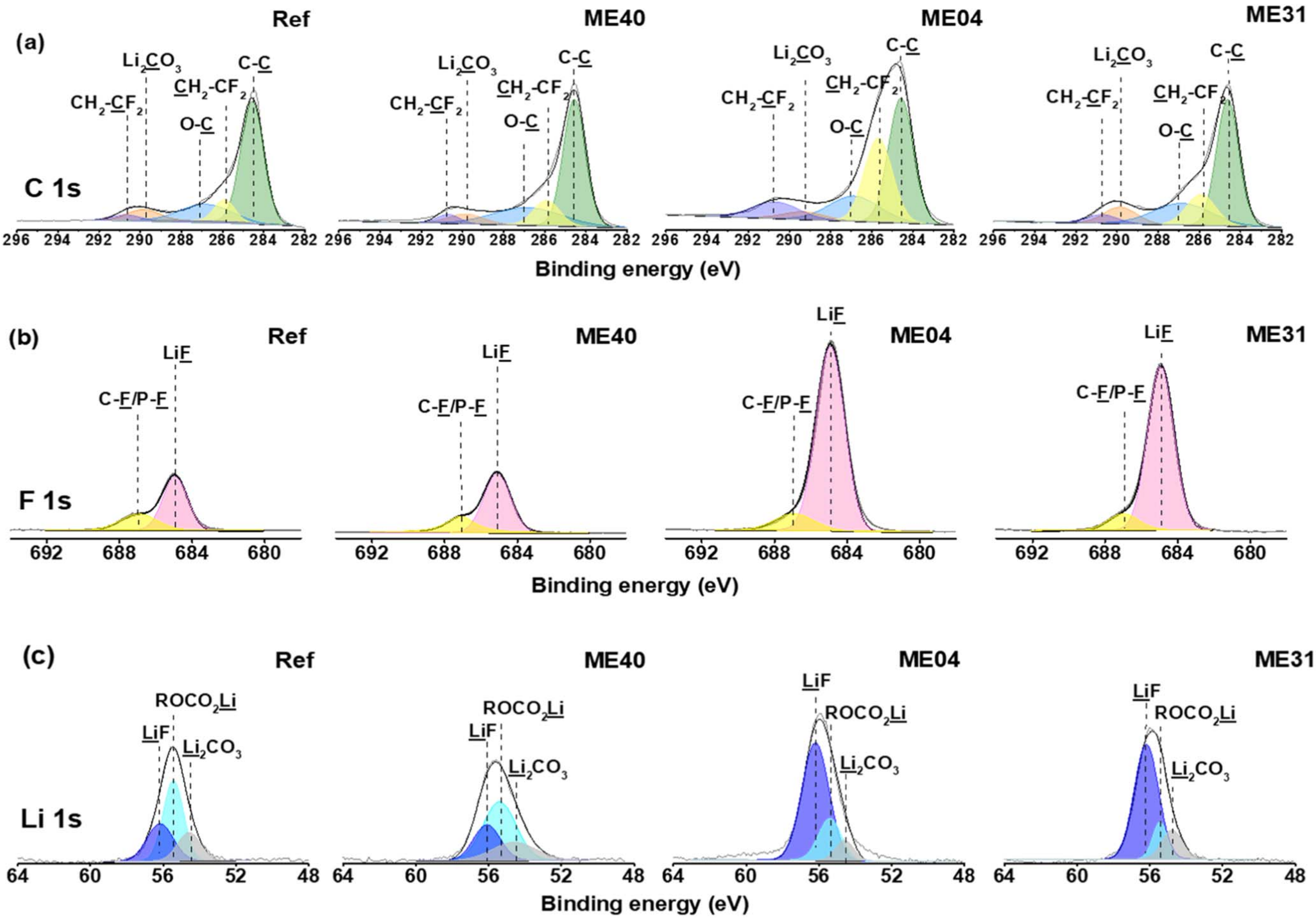

Figure 4. (a) C 1 s, (b) F 1 s, and (b) Li 1 s XPS spectra of the graphite anodes after two pre-conditioning cycles.

among organic solvents (EC, EMC, MA, and EFA) in the electrolyte, which was consistent with Raman and ^{7}Li NMR results. Based on the Raman and ^{7}Li NMR analyses, the variation of solvation structure with the addition of EFA is schematically presented in Fig. 3e. The addition of EFA increases the Li^+-coordinated PF_6^- solvation, leading the participation of anions in the formation of SEI layer on the graphite anode. In addition, the weakened interactions between the Li^+ ions and the solvents facilitate the de-solvation of Li^+ ions, reducing the charge transfer resistance under low-temperature operations.

To analyze the chemical composition of the SEI layer formed on the graphite anode, XPS spectra were obtained after two pre-conditioning cycles of the cell. In the C 1 s XPS spectra, ME04 exhibited the highest peak intensity of CH_2-CF_2 at 285.9 and 290.7 eV, which can be ascribed the reductive decomposition of the EFA solvent. In the F1s XPS spectra of Fig. 4b, the peaks at 685.1 and 687.2 eV correspond to LiF and C-F/P-F, respectively, which arose from the decomposition of the PF_6^- anion and PVdF binder.[43,44] The ME04 and ME31 showed higher LiF peak intensities than Ref and ME40, indicating that the PF_6^- anions in the solvation structure were reductively decomposed on the graphite anode. The LiF-based SEI is mechanically robust and stable, which can enhance cycling stability.[36,45] The Li 1 s XPS spectra in Fig. 4c could be resolved into three primary peaks centered at 54.7, 55.4, and 56.2 eV, corresponding to Li_2CO_3, $ROCO_2Li$, and LiF, respectively.[44,46,47] The peak intensities of Li_2CO_3 and lithium alkoxides (RO-Li) corresponding to the decomposition products of carbonate solvents were reduced in the ME04 and ME31 electrolytes. These results suggest that the addition of EFA promotes the formation of inorganic-rich SEI layer rather than an organic-based SEI on the graphite anode, highlighting the beneficial role of EFA, as schematically explained in Fig. 1.

The cycling performance of the graphite/LFP cells with different electrolytes was evaluated at −20 °C. Prior to low-temperature cycling, the cell was subjected to two pre-conditioning cycles at 0.1 C and 20 pre-cycles at 1.0 C and 25 °C to form a stable interphase layer and stabilize the cell. As shown in Fig. S3, all the cells exhibited stable cycling behavior, delivering the discharge capacities ranging from 126 to 131 mA g^{-1} at 1.0 C and 25 °C. Subsequently, the cell was charged to 3.9 V at 0.2 C and 25 °C and discharged to 2.5 V at 0.2 C and −20 °C. The resulting discharge curves are presented in Fig. 5a. When compared with room-temperature cycling (Fig. S3), the discharge capacities were significantly reduced at −20 °C. The cells assembled with electrolyte containing cosolvents delivered higher discharge capacities than the cell with Ref, and the cell with a dual cosolvent (ME31) exhibited the highest discharge capacity. The galvanostatic cycling of the cells was conducted at 0.33 C and −20 °C. The cycling curves of the cells employing different electrolytes are presented in Figs. 5b and S4. The low-temperature cycling performance of the cells is compared in Fig. 5c and Table S2. It can be seen that the cell with ME31 exhibited the best cycling performance in terms of initial discharge capacity and cycling stability at −20 °C. This result can be attributed to the synergistic effect of MA and EFA, because MA exhibited high ionic conductivity and low viscosity at low temperatures, while maintaining the solvation structure change due to the presence of EFA. In contrast, the cell employing Ref delivered the lowest initial discharge capacity with poor capacity retention. This is because the

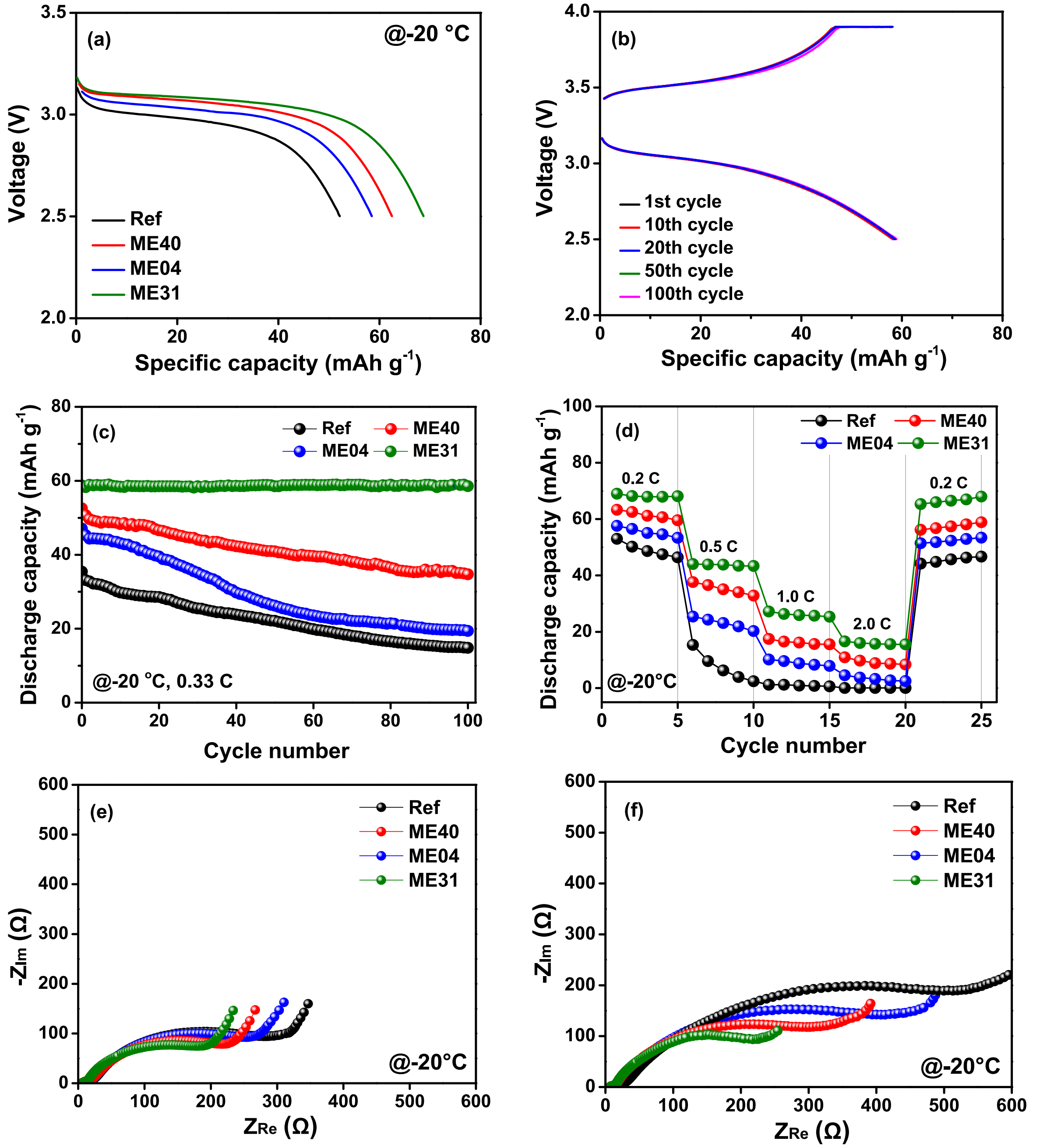

Figure 5. (a) First discharge curves of the cells with different electrolytes at 0.2 C and −20 °C. (b) Voltage profiles of the cell with ME31 at 0.33 C and −20 °C. (c) Cycling performance of the cells with different electrolytes at −20 °C with 0.33 C. (d) Rate capability of the cells with varying electrolytes at −20 °C. AC impedance spectra of the cells with varying electrolytes after (e) pre-conditioning and (f) 100 cycles at −20 °C.

cell with Ref has low ionic conductivity and large charge transfer resistance due to the difficult Li^+ de-solvation at low temperatures. These presumptions could be confirmed by the electrochemical impedance measurements of the cells with different electrolytes at −20 °C. Figures 5e and 5f show the AC impedance spectra of the cell varying electrolyte after pre-conditioning and 100 cycles at −20 °C, respectively. We fitted the experimental data using an equivalent circuit in Fig. S5, and the results are summarized in Table S3. In the equivalent circuit, R_e is the resistance of electrolyte, R_f is the resistance associated with the surface film formed on the electrode, and R_{ct} is the charge transfer resistance at the electrode-electrolyte interface. The cell employing ME31 showed the lowest interfacial resistances (R_f and R_{ct}) after pre-conditioning and 100 cycles, which resulted from the formation of stable anion-derived SEI layer and low de-solvation energy. These results can be attributed to the synergistic effect of MA and EFA, as explained earlier. MA improves the Li^+ ion transport by lowering the viscosity at low temperatures, while EFA reduces the charge transfer resistance by lowering the de-solvation energy and forming an inorganic-rich thin SEI layer. In contrast, the cell using conventional electrolyte (Ref) exhibited the largest electrolyte and interfacial resistances, consistent with low-temperature cycling characteristics. When comparing the rate capability of the cells at −20 °C in Fig. 5d, the cell with ME31 revealed a superior high rate performance than other cells, indicating that the addition of a dual cosolvent (MA and EFA) with an optimum ratio rather than a single cosolvent (MA or

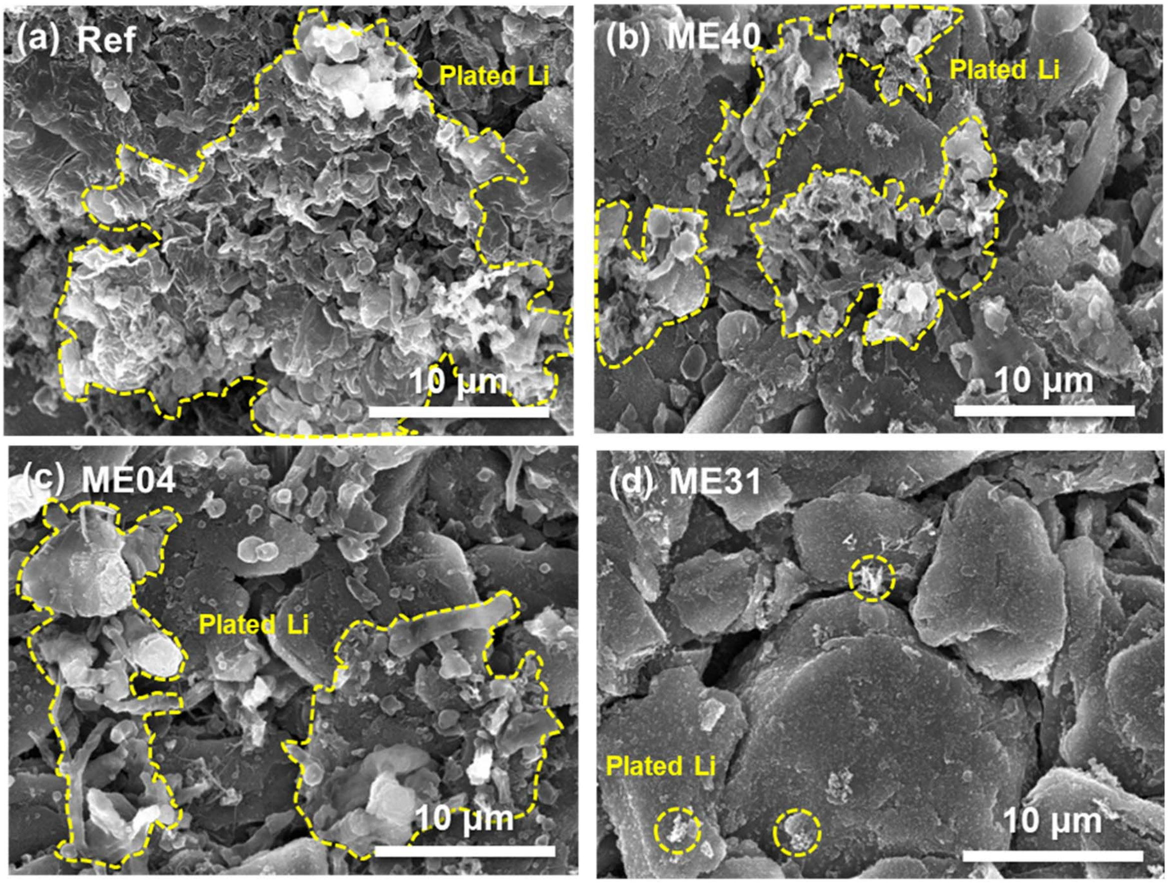

Figure 6. SEM images of graphite anodes disassembled from the graphite/LFP cells employing (a) Ref, (b) ME40, (c) ME04, and (d) ME31 after 100 cycles at −20 °C.

EFA) more effectively improved the rate capability at low temperatures due to their synergistic effect. The cycle test of the cells was identically conducted at −30 °C, and the results are presented in Fig. S6 and Table S2. Although all the cells showed cycling performance worse than that at −20 °C, the cell employing ME31 still exhibited the best cycling performance at −30 °C, consistent with the results obtained at −20 °C.

Surface SEM images of the graphite anodes after 100 cycles at −20 °C are shown in Fig. 6 and Fig. S7. When examining the SEM images of pristine graphite anode before cycling (Fig. S8), the surface of active materials was clean without any coverage. However, the graphite anodes after cycling are covered with side products and plated lithium, as shown in Fig. 6. Notably, significant amounts of plated lithium could be observed on the surface of graphite anode cycled in Ref electrolyte, indicating that difficult de-solvation and slow transport of Li^+ ions through the SEI in Ref electrolyte caused severe Li plating on the graphite anode during charge process under low-temperature conditions.[48,49] In the ME40 and ME04 electrolytes with a single cosolvent, lithium was also partially plated on the active material. In contrast, the surface of the graphite anode cycled in ME31 remained clean and only small amounts of plated lithium could be observed. These results suggest that ME31 with low viscosity and facile de-solvation restricts only to a small extent the intercalation of Li^+ ions into the anode even at low temperatures, resulting in less lithium plating.

Finally, the long-term cycling performance of the cells was evaluated at 25 °C and 1.0 C rate to confirm that the electrolyte optimized for low temperatures also exhibited good cycling performance at room temperature. As presented in Fig. 7a, the cell employing ME31 exhibited quite stable voltage profiles with an initial discharge capacity of 131.2 mAh g^{-1}. The discharge capacities gradually increased with cycling during earlier cycles (Fig. 7b), which can be ascribed to the stabilization of electrodes upon cycling. After 300 cycles, the cell showed a high capacity retention of 99.4% with respect to its first discharge capacity. From the rate capability test in Fig. 7c, the cell employing ME31 showed good high-rate performance, delivering a high discharge capacity of 95.3 mAh g^{-1} at 5.0 C rate. These results reveal that the liquid electrolytes using dual cosolvents (MA and EFA) with an optimal ratio can be promising electrolyte systems for achieving good cycling performance at both low and room temperatures.

Conclusions

This study proposes an electrolyte system containing a dual cosolvent to enhance the low-temperature cycling performance of the lithium-ion cells. The dual cosolvent was composed of MA and EFA to complement the limitations of esters and fluorinated esters while maintaining their advantages. The dual cosolvent effectively reduced the de-solvation energy, while maintaining high ionic conductivity at low temperatures. Additionally, it facilitated the formation of a robust, stable, and inorganic-rich SEI layer by altering the solvation structure. The graphite/LFP cell employing an optimized dual cosolvent exhibited superior cycling performance compared to the cells using conventional electrolytes or electrolytes containing single cosolvents at low temperatures due to their synergistic effect. Our results provide valuable insights into the

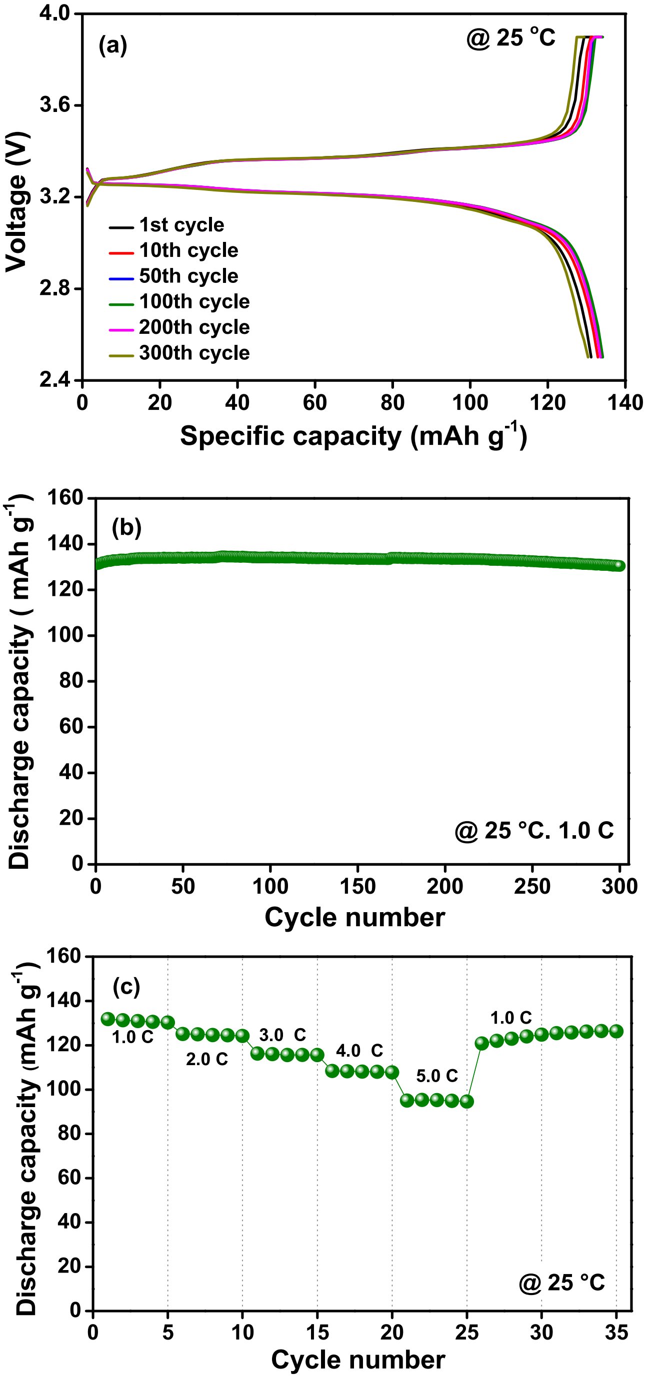

Figure 7. (a) Voltage profiles and (b) cycling performance of the cell assembled with ME31 at 1.0 C and 25 °C. (c) Rate capability of the cell with ME31 at 25 °C.

design principles for new electrolytes that can efficiently operate under low-temperature environments.

Acknowledgments

This work was supported by the Technology Innovation Program (20024252), funded by the Ministry of Trade, Industry, and Energy (MOTIE, Korea).

ORCID

Jin-Young Oh https://orcid.org/0009-0008-3220-221X
Dong-Won Kim https://orcid.org/0000-0002-1735-0272

References

1. J.-M. Tarascon and M. Armand, "Issues and challenges facing rechargeable lithium batteries." *Nature*, **414**, 359 (2001).
2. M. R. Palacin, "Recent advances in rechargeable battery materials: a chemist's perspective." *Chem. Soc. Rev.*, **38**, 2565 (2009).
3. B. Scrosati, J. Hassoun, and Y.-K. Sun, "Lithium-ion batteries. a look into the future." *Energy Environ. Sci.*, **4**, 3287 (2011).
4. R. Schmuch, R. Wagner, G. Horpel, T. Placke, and M. Winter, "Performance and cost of materials for lithium-based rechargeable automotive batteries." *Nat. Energy*, **3**, 267 (2018).
5. M. Li, J. Lu, Z. Chen, and K. Amine, "30 Years of lithium-ion batteries." *Adv. Mater.*, **30**, 1800561 (2018).
6. Z. Cano, D. Banham, S. Ye, A. Hintennach, J. Lu, M. Fowler, and Z. Chen, "Batteries and fuel cells for emerging electric vehicle markets." *Nat. Energy*, **3**, 279 (2018).
7. S. Zhang, T. Jow, K. Amine, and G. Henriksen, "$LiPF_6$–EC–EMC electrolyte for Li-ion battery." *J. Power Sources*, **107**, 18 (2002).
8. K. Xu, "Li-ion battery electrolytes." *Nat. Energy*, **6**, 763 (2021).
9. D. Hubble, D. E. Brown, Y. Zhao, C. Fang, J. Lau, B. D. McCloskey, and G. Liu, "Liquid electrolyte development for low-temperature lithium-ion batteries." *Energy Environ. Sci.*, **15**, 550 (2022).
10. D.-J. Yoo, Q. Liu, O. Cohen, M. Kim, K. A. Persson, and Z. Zhang, "Understanding the role of SEI layer in low-temperature performance of lithium-ion batteries." *ACS Appl. Mater. Interfaces*, **14**, 11910 (2022).
11. M. Ding, K. Xu, S. Zhang, K. Amine, G. Henriksen, and T. Jow, "Change of conductivity with salt content, solvent composition, and temperature for electrolytes of $LiPF_6$ in ethylene carbonate-ethyl methyl carbonate." *J. Electrochem. Soc.*, **148**, A1196 (2001).
12. S. Zhang, K. Xu, and T. Jow, "The low temperature performance of Li-ion batteries." *J. Power Sources*, **115**, 137 (2003).
13. S. S. Zhang, K. Xu, and T. R. Jow, "Electrochemical impedance study on the low temperature of Li-ion batteries." *Electrochim. Acta*, **49**, 1057 (2004).
14. Q. Li, D. Lu, J. Zheng, S. Jiao, L. Luo, C.-M. Wang, K. Xu, J.-G. Zhang, and W. Xu, "Li+-desolvation dictating lithium-ion battery's low-temperature performances." *ACS Appl. Mater. Interfaces*, **9**, 42761 (2017).
15. Q. Li, G. Liu, H. Cheng, Q. Sun, J. Zhang, and J. Ming, "Low-temperature electrolyte design for lithium-ion batteries: Prospect and challenges." *Chem. Eur. J.*, **27**, 15842 (2021).
16. L. Chen, H. Wu, X. Ai, Y. Cao, and Z. Chen, "Toward wide-temperature electrolyte for lithium–ion batteries." *Battery Energy*, **1**, 20210006 (2022).
17. W. Xue, T. Qin, Q. Li, M. Zan, X. Yu, and H. Li, "Exploiting the synergistic effects of multiple components with a uniform design method for developing low-temperature electrolytes." *Energy Storage Mater.*, **50**, 598 (2022).
18. N. Zhang, T. Deng, S. Zhang, C. Wang, L. Chen, C. Wang, and X. Fan, "Critical review on low-temperature Li-ion/metal batteries." *Adv. Mater.*, **34**, 2107899 (2022).
19. W. Lin, M. Zhu, Y. Fan, H. Wang, G. Tao, M. Ding, N. Liu, H. Yang, J. Wu, and J. Fang, "Low temperature lithium-ion batteries electrolytes: rational design, advancements, and future perspectives." *J. Alloys Compd.*, **905**, 164163 (2022).
20. M. Qin, Z. Zeng, Q. Wu, X. Liu, Q. Liu, S. Cheng, and J. Xie, "1,3,5-Trifluorobenzene endorsed EC-free electrolyte for high-voltage and wide-temperature lithium-ion batteries." *J. Energy Chem.*, **85**, 49 (2023).
21. L. Luo, K. Chen, H. Chen, H. Li, R. Cao, X. Feng, W. Chen, Y. Fang, and Y. Cao, "Enabling ultralow-temperature (–70 °C) lithium-ion batteries: advanced electrolytes utilizing weak-solvation and low-viscosity nitrile cosolvent." *Adv. Mater.*, **36**, 2308881 (2024).
22. D. J. Yoo, Q. Liu, O. Cohen, M. Kim, K. A. Persson, and Z. Zhang, "Rational design of fluorinated electrolytes for low temperature lithium-ion batteries." *Adv. Energy Mater.*, **13**, 2204182 (2023).
23. Y. Ein-Eli, S. Thomas, R. Chadha, T. Blakley, and V. Koch, "Li-ion battery electrolyte formulated for low-temperature applications." *J. Electrochem. Soc.*, **144**, 823 (1997).
24. S. V. Sazhin, M. Y. Khimchenko, Y. N. Tritenichenko, and H. S. Lim, "Performance of Li-ion cells with new electrolytes conceived for low-temperature applications." *J. Power Sources*, **87**, 112 (2000).
25. S. Herreyre, O. Huchet, S. Barusseau, F. Perton, J. M. Bodet, and P. Biensan, "New Li-ion electrolytes for low temperature applications." *J. Power Sources*, **97-98**, 576 (2001).
26. M. C. Smart, B. V. Ratnakumar, and S. Surampudi, "Use of organic esters as cosolvents in electrolytes for lithium-ion batteries with improved low temperature performance." *J. Electrochem. Soc.*, **149**, A361 (2002).
27. M. C. Smart, B. V. Ratnakumar, K. B. Chin, and L. D. Whitcanack, "Lithium-ion electrolytes containing ester cosolvents for improved low temperature performance." *J. Electrochem. Soc.*, **157**, A1361 (2010).
28. K. Chen, Z. Yu, S. Deng, Q. Wu, J. Zou, and X. Zeng, "Evaluation of the low temperature performance of lithium manganese oxide/lithium titanate lithium-ion batteries for start/stop applications." *J. Power Sources*, **278**, 411 (2015).
29. Y. G. Cho, M. Li, J. Holoubek, W. Li, Y. Yin, Y. S. Meng, and Z. Chen, "Enabling the low-temperature cycling of NMC‖graphite pouch cells with an ester-based electrolyte." *ACS Energy Lett.*, **6**, 2016 (2021).
30. H.-C. A. Shiao, D. Chua, H.-P. Lin, S. Slane, and M. Salomon, "Low temperature electrolytes for Li-ion PVDF cells." *J. Power Sources*, **87**, 167 (2000).
31. M. Smart, B. Ratnakumar, V. Ryan-Mowrey, S. Surampudi, G. Prakash, J. Hu, and I. Cheung, "Improved performance of lithium-ion cells with the use of fluorinated carbonate-based electrolytes." *J. Power Sources*, **119**, 359 (2003).

32. K. Xu, "Electrolytes and interphases in Li-ion batteries and beyond." *Chem. Rev.*, **114**, 11503 (2014).
33. J. Li, H. Li, X. Ma, W. Stone, S. Glazier, E. Logan, E. M. Tonita, K. L. Gering, and J. Dahn, "Methyl acetate as a co-solvent in NMC532/graphite cells." *J. Electrochem. Soc.*, **165**, A1027 (2018).
34. K. An, Y. H.-T. Tran, S. Kwak, J. Han, and S. W. Song, "Design of fire-resistant liquid electrolyte formulation for safe and long-cycled lithium-ion batteries." *Adv. Funct. Mater.*, **31**, 2106102 (2021).
35. Y. Yang, P. Li, N. Wang, Z. Fang, C. Wang, X. Dong, and Y. Xia, "Fluorinated carboxylate ester-based electrolyte for lithium-ion batteries operated at low temperature." *Chem. Commun.*, **56**, 9640 (2020).
36. S.-J. Kang, K. Park, S.-H. Park, and H. Lee, "Unraveling the role of LiFSI electrolyte in the superior performance of graphite anodes for Li-ion batteries." *Electrochim. Acta*, **259**, 949 (2018).
37. J.-W. Kim, M.-K. Oh, Y.-A. Kim, U. T. Nakate, E.-J. Kwon, S. Seo, W.-K. Kim, K.-H. Ryu, and D.-W. Kim, "Enhanced cycle life of lithium metal batteries via modulating the lithium-ion solvation sheath with a cross-linked gel polymer electrolyte." *J. Power Sources*, **598**, 234183 (2024).
38. P. Ma, P. Mirmira, and C. V. Amanchukwu, "Effect of building block connectivity and ion solvation on electrochemical stability and ionic conductivity in novel fluoroether electrolytes." *ACS Cent. Sci*, **7**, 1232 (2021).
39. T. Wang, R. Wan, Z. Tang, J. W. Yap, J. Shao, L. Qin, S. Zhang, J. Choi, Y. Wu, and J. H. Kim, "Dual-salts localized high-concentration electrolyte for Liand Mn-Rich high-voltage cathodes in lithium metal batteries." *Small*, 2401364 (2024).
40. P. Nie, M. Liu, W. Qu, M. Hou, L. Chang, Z. Wu, H. Wang, and J. Jiang, "Unravelling the solvation structure and interfacial mechanism of fluorinated localized high concentration electrolytes in K-ion batteries." *Adv. Funct. Mater.*, **33**, 2302235 (2023).
41. G. Song, Z. Yi, F. Su, L. Xie, Z. Wang, X.-X. Wei, G. Xu, and C.-M. Chen, "Boosting the low-temperature performance for Li-ion batteries in $LiPF_6$-based local high-concentration electrolyte." *ACS Energy Lett.*, **8**, 1336 (2023).
42. S. Yuan, S. Cao, X. Chen, J. Wei, Z. Lv, H. Xia, J. Li, H. Zhang, L. Liu, and C. Tian, "Deshielding anions enable solvation chemistry control of $LiPF_6$-based electrolyte toward low-temperature lithium-ion batteries." *Adv. Mater.*, **36**, 2311327 (2024).
43. D.-A. Lim, J.-H. Seok, D. Hong, K. H. Ahn, C. H. Lee, and D.-W. Kim, "Non-flammable gel polymer electrolyte for enhancing safety and high-temperature performance of lithium-ion batteries." *ACS Appl. Mater. Interfaces*, **16**, 14822 (2024).
44. F. Wu, A. R. Schur, G.-T. Kim, X. Dong, M. Kuenzel, T. Diemant, G. D'Orsi, E. Simonetti, M. De Francesco, and M. Bellusci, "A novel phosphonium ionic liquid electrolyte enabling high-voltage and high-energy positive electrode materials in lithium-metal batteries." *Energy Storage Mater.*, **42**, 826 (2021).
45. B. Nan, L. Chen, N. D. Rodrigo, O. Borodin, N. Piao, J. Xia, T. Pollard, S. Hou, J. Zhang, and X. Ji, "Enhancing Li^+ transport in NMC811||graphite lithium-ion batteries at low temperatures by using low-polarity-solvent electrolytes." *Angew. Chem. Int. Ed.*, **61**, e202205967 (2022).
46. D. J. Lee, H. Lee, Y. J. Kim, J. K. Park, and H. T. Kim, "Sustainable redox mediation for lithium-oxygen batteries by a composite protective layer on the lithium-metal anode." *Adv. Mater.*, **28**, 857 (2016).
47. X. Q. Zhang, X. Chen, X. B. Cheng, B. Q. Li, X. Shen, C. Yan, J. Q. Huang, and Q. Zhang, "Highly stable lithium metal batteries enabled by regulating the solvation of lithium ions in nonaqueous electrolytes." *Angew. Chem.*, **130**, 5275 (2018).
48. S. S. Zhang, K. Xu, and T. R. Jow, "A new approach toward improved low temperature performance of Li-ion battery." *Electrochem. Commun.*, **4**, 928 (2002).
49. J. Qin, Q. Lan, N. Liu, Y. Zhao, Z. Song, and H. Zhan, "A metal-free battery working at –80 °C." *Energy Storage Mater.*, **26**, 585 (2020).